Atmos. Chem. Phys. Discuss., 12, 11567–11594, 2012
www.atmos-chem-phys-discuss.net/12/11567/2012/
doi:10.5194/acpd-12-11567-2012


Atmospheric Chemistry and Physics Discussions



# Height increase of the melting level stability anomaly in the tropics

**I. Folkins**

Department of Physics and Atmospheric Science, Dalhousie University Halifax, B3H 3J5, Nova Scotia, Canada

Received: 9 February 2012 – Accepted: 18 April 2012 – Published: 4 May 2012

Correspondence to: I. Folkins (ian.folkins@dal.ca)

Published by Copernicus Publications on behalf of the European Geosciences Union.







## Abstract

In actively convecting regions of the tropics, the lower troposphere is significantly less stable than predicted by a moist pseudoadiabat. This anomalous variation in lapse rate occurs between the boundary layer inversion (∼2 km) and the melting level (∼5 km), and has been attributed to mesoscale downdrafts that develop below precipitating stratiform anvil clouds. We use an 11 yr record (1998–2008) from five Western Tropical Pacific radiosonde stations in the Stratospheric Processes and their Role in Climate (SPARC) archive, to determine the response of this stability anomaly to changes in monthly mean surface temperature. We find that the stability anomaly shifts upward when the surface temperature increases, by an amount roughly equal to the upward displacement of the melting level. It is likely that this change in lower tropospheric stability is associated with increases in the height of cumulus congestus clouds, in the vertical distance through which stratiform precipitation falls through cloud free air, and in the vertical wavelength of the stratiform heating mode.

## 1 Introduction

Within a precipitating stratiform anvil cloud, the rate of ice crystal aggregation increases as ice crystals descend toward the melting level. The resulting acceleration in fall speed (Tokay et al., 1999) increases the downward flux of ice condensate. When the ice particles (mostly snow) fall below the 0 °C level and melt into raindrops, there is a further increase in fall speed. In the absence of a mesoscale uplift below the melting level sufficient to generate new cloud droplets, cloud microphysical processes should therefore constrain the base of precipitating stratiform anvil clouds to an altitude near the melting level (Houze, 2004).

In the tropics, the height of the melting level has been rising for the past several decades (Bradley et al., 2009). This would be expected to increase the vertical distance through which stratiform precipitation evaporates as it falls through cloud free air below





ACPD
12, 11567–11594, 2012



the melting level. This increase in cloud free fall distance, and the fact that the raindrops will fall through a warmer atmosphere with a larger saturation vapour pressure near the surface, should decrease the precipitation efficiency of stratiform precipitation.

The condensation of water vapor into supercooled water, and the freezing of supercooled water into ice, contribute to mesoscale heating and ascent within a precipitating stratiform anvil cloud. Below precipitating stratiform anvil clouds, the melting of ice and evaporation of water contribute to mesoscale cooling and descent. The resulting heating dipole (upper tropospheric heating and lower tropospheric cooling) is referred to as the stratiform heating mode. Some of the equatorially trapped waves generated by this heating profile are strongly coupled to moist convection, and generate rainfall disturbances which propagate parallel to the equator (Mapes and Houze, 1995; Kiladis et al., 2009). If the mean stratiform cloud base shifts to a higher altitude in a warmer climate, the vertical wavelength of the stratiform heating mode will increase. This increase would be expected to increase the propagation speed of both the waves generated by this mode and their associated rainfall anomalies.

One way to obtain indirect insight into the changes in stratiform precipitation efficiency and rainfall variance, expected to occur in association with an increase in the mean stratiform cloud base height, is to examine how the stability of the lower troposphere changes in response to changes in surface temperature. The temperature profile in actively convecting regions of the tropics is often considered to be moist adiabatic or pseudoadiabatic. In the lower troposphere, however, the climatological lapse rate exhibits significant deviations from a moist pseudoadiabatic profile (Mapes, 2001). In the current atmosphere, these deviations occur between the top of the boundary layer ($\sim 2$ km) and the 0 °C melting level ($\sim 5$ km), and have been referred to as the Melting Level Stability Anomaly (MLSA) (Folkins, 2009). Although the physical origin of the MLSA has not been definitively established, it has been attributed to a rapid increase in the stratiform downdraft mass flux, as stratiform precipitation enters cloud free air below the melting level (Folkins, 2009). In this case, the MLSA would be expected to shift upward in response to an increase in surface temperature. In this paper,





ACPD
12, 11567–11594, 2012



we use radiosonde data to show that the MLSA does indeed shift to a higher altitude when the surface temperature increases. This upward shift is roughly equal to that required to keep the upper boundary of the MLSA near the melting level.

A vertical shift in the MLSA should modify the detrainment profile of some convective clouds. Cumulus congestus clouds are responsible for roughly 30 % of tropical precipitation (Johnson et al., 1999), and influence the distribution of chemical tracers such as ozone (Mitovski et al., 2012). Outflow from these clouds preferentially detrains near layers of enhanced stability at the top of the MLSA (Johnson et al., 1999; Redelsberger et al., 2002). In a warmer atmosphere, in which the melting level occurred at a higher altitude, the outflow from cumulus congestus clouds should also shift to a higher altitude.

Temperature profiles from radiosondes are usually not archived with sufficient vertical resolution to characterize the complex variation of lapse rate with height in the tropical lower troposphere. They also often suffer from instrumental biases which introduces uncertainties into the calculation of trends in lapse rate (Sherwood et al., 2005; Randel and Wu, 2006; Thorne et al., 2011). Here, we use an 11 yr year record (1998–2008) of homogeneous, high vertical resolution radiosonde measurements from five stations in the Western tropical Pacific, to examine the response of the tropical atmosphere to changes in surface temperature.

In the tropics, the timescale to reach radiative convective equilibrium (and the convective overturning timescale), is roughly equal to a month (Emanuel, 1994). The timescale over which temperatures in the free troposphere come into equilibrium with temperature fluctuations near the surface should also roughly equal a month. The twice daily radiosonde measurements were therefore used to calculate monthly mean temperature profiles at each site. Monthly means from the entire 11 yr period (1998–2008) were then used to define the vertical profile of the monthly temperature anomaly at each site. The monthly anomalies of the five radiosonde sites were then averaged together, and used to calculate the vertical profile of the regional temperature response





ACPD
12, 11567–11594, 2012



to changes surface temperature (defined here as the average temperature below 1 km) on monthly timescales.

The vertical structure of the response to changes in near surface temperature that occur on monthly timescales is unlikely to exactly equal the response to changes in near surface temperature that occur on longer timescales. However, we use temperature profiles from the World Climate Research Programme's (WCRP's) Coupled Model Intercomparison Project phase 3 (CMIP3) multi-model dataset (Meehl et al., 2007) to show that the monthly timescale response obtained from an 11 yr record should be similar to the response obtained from a longer term record.

## 2 Datasets

### 2.1 Radiosondes

The radiosonde data were taken from the Stratospheric Processes and their Role in Climate (SPARC) radiosonde archive. We used 1998–2008 data from Koror (Palau Island: 7.33° N, 134.48° E), Yap Island (9.48° N, 138.08° E). Truk (Moen Island: 7.47° N, 151.85° E), Ponape Island (6.97° N, 158.22° E), and Majuro (Marshall Island: 7.08° N, 171.38° E), The twice daily measurements were used to construct monthly mean profiles of temperature, pressure, and relative humidity on a 200 m vertical grid. The five radiosonde stations occur in a roughly linear sequence parallel to the equator stretching eastward from the Philippines, and are located within the northern branch of the Inter-Tropical Convergence Zone. At each station, maximum rainfall usually occurs in July or August, with maximum rain rates of 8–12 mm day$^{-1}$. Monthly mean rain rates at the five stations almost always exceeds 3 mm day$^{-1}$, so that none of the stations ordinarilly exhibit a dry season.





ACPD
12, 11567–11594, 2012



## 2.2 Rainfall

In the absence of moist convection, the free troposphere becomes decoupled from the boundary layer, and the correlation between temperature anomalies at the surface and upper levels should disappear. We have therefore filtered the radiosonde data to remove months in which the mean rainfall rate fell below a particular threshold. Monthly mean rain rates were determined from the Tropical Rainfall Measuring Mission (TRMM) 3B42 gridded dataset, which contains rainfall estimates on a 0.25° grid every 3 h (Kummerow et al., 2000). The average rain rate in a 2° × 2° box, centered at each of the five radiosonde locations, was determined for each month between 1998 and 2008.

## 2.3 Climate models

We used monthly mean output fields from six coupled ocean-atmosphere models participating in the CMIP 3 Climate of the Twentieth Century Experiment. The forcing agents used in this experiment include greenhouse gases ($CO_2$, $CH_4$, $N_2O$, and CFC's), direct effects from sulfate aerosols, volcanoes, and solar forcings. The simulations usually start in 1850. We used 1950–2000 output from the following six models: (i) Canadian Centre for Climate Modelling and Analysis CGCM3 (CCCMA CGCM3, 3.75° × 3.75° horizontal resolution), (ii) National Center for Atmospheric Research CCSM3 (NCAR CCSM3, 1.4° × 1.4° horizontal resolution), (iii) Hadley Centre for Climate Prediction and Research HADCM3 (UKMO HADCM3, 3.75° × 2.5° horizontal resolution), (iv) CSIRO Atmospheric Research MK3 (CSIRO MK3, 1.875° × 1.875° horizontal resolution), (v) Goddard Institute for Space Studies MODEL E H (GISS MODEL E H, 5.0° × 4.0° horizontal resolution), and (vi) Centre National de Recherches Météorologiques CM3 (CNRM CM3, 2.81° × 2.81° horizontal resolution). All models have 17 vertical levels, except the UKMO model which has 15. Typically, 12 of these levels are in the troposphere (below 17 km). Monthly mean temperature profiles from





ACPD
12, 11567–11594, 2012



these simulations were analyzed using the same procedures used for the radiosonde data.

## 3 Results

### 3.1 Observed lapse rate

The solid black line in Fig. 1 shows the lapse rate profile obtained by averaging all monthly mean temperature profiles from the five radiosonde locations. This profile illustrates the trimodal character of tropical convective outflow (Johnson et al., 1999). The local stability maxima at 2 km and 5.5 km are associated with preferred detrainment from boundary layer and cumulus congestus clouds. The rapid increase in stability above 13 km is associated with detrainment from deep convection.

The dashed line in Fig. 1 shows the lapse rate generated by subjecting an air parcel at the surface with a temperature of 299.5 K and relative humidity of 80 %, to pseudoadiabatic ascent. During pseudoadiabatic ascent, all condensate is assumed to produce precipitation and is immediately removed. The maximum permitted vapor pressure was set equal to the saturation vapor pressure over water for temperatures larger than 0 °C, and to the saturation vapor pressure over ice for temperatures less than 0 °C. This change to a more rapid decrease in saturation vapor pressure at the melting level increases the rate of condensational heating in the rising air parcel. This generates a slightly more stable lapse rate, and gives rise to the small notch in the lapse rate at the melting level shown in Fig. 1.

Between 6 km and 10 km, the observed lapse rate approximates a moist pseudoadiabat. Between the top of the boundary level (∼ 2 km) and the melting level (∼ 5 km), the lapse rate varies with altitude in a complex manner that is not usefully described as either a moist pseudoadiabat or reversible adiabat (Mapes, 2001; Folkins, 2006).





ACPD
12, 11567–11594, 2012



### 3.2 Rain based filtering

In the tropics, rainfall anomalies generate temperature anomalies with a spatial range of roughly 1000 km in the lower troposphere, and 2000 km in the upper troposphere (Folkins et al., 2008). In actively convecting regions, the correlation between monthly temperature anomalies at a common height between nearby radiosonde stations should decay with a similar spatial scale. The correlation between the monthly temperature anomalies of Koror and Yap, between 1998 and 2008, is shown in Fig. 2 using a dark line. Koror and Yap are separated by a distance of less than 500 km, and their temperature anomalies are strongly correlated at all heights, with the exception of a layer near the surface, and another layer near the top of the boundary layer. Figure 2 also shows the vertical variation of the correlation between Koror and the other three radiosonde locations. In the troposphere, the strength of the correlation between two stations decreases as their separation increases.

The black dots in Fig. 3 show the temperature anomalies of the 200 m layer nearest 10 km plotted against the near surface (below 1 km) temperature anomalies, averaged over the five radiosonde stations, and using every month from 1998 to 2008. The surface temperature anomalies are typically less than −0.4 °C, and are positively correlated with temperature anomalies at 10 km.

In the absence of moist convection, temperatures in the free troposphere should become decoupled from temperatures near the surface. The gray dots in Fig. 3 denote site average temperature anomalies in which the mean rainfall rate in a 2.0° × 2.0° box centered at the radiosonde stations was less than 3.0 mm per day, for at least three of the five stations. This situation occurred, for example, during the first four months of 1998, when a strong El Nino gave rise to a large rainfall enhancement in the Central Pacific (Adler et al., 2000), to the east of the five radiosonde locations. The large scale upper tropospheric warming (Chiang and Lintner, 2005) associated with this rainfall enhancement, and local reductions in sea surface temperature (McPhaden, 1999), contributed to a reduction in rainfall over the radiosonde region during the first four





ACPD
12, 11567–11594, 2012



months of 1998. This rainfall reduction accounts for the decoupling between the near surface and 10 km temperature anomalies that occurred during the first four months of 1998.

The strength of the coupling between near surface and upper tropospheric temperature anomalies depends on the local rain rate. The monthly mean near surface (< 1 km) and upper tropospheric (10 km) temperature anomalies of a particular radiosonde location were assigned to a particular bin based on the average rain rate for that month. A correlation coefficient was then calculated using all temperature anomaly pairs from a common rain bin. Figure 4 shows that for rain rates less than 2 mm per day, upper tropospheric temperature anomalies are negatively correlated with near surface temperature anomalies. For rain rates larger than 2 mm per day, the correlation initially increases with rain rate, but then reaches a limiting value of roughly 0.5 for rain rates larger than 6 mm day$^{-1}$. Due to the exponential decrease in the frequency of occurrence of high rain rates, the correlation coefficient becomes increasingly statistically uncertain for monthly mean rain rates in excess of 12 mm per day.

### 3.3 Observed amplification factor

Figure 5 shows the vertical profile of the temperature response that would be expected from a 1 °C increase in the site average near surface temperature. This response, or "amplification factor", was calculated from the slope of a scatter-plot of the site average temperature anomaly at each height against the site average near surface temperature anomaly. Time periods in which the anomalies become decoupled were removed by using only those months in which the monthly rain rate exceeded 3 mm per day for at least three of the five radiosonde locations (corresponding to the open circles in Fig. 3). The amplification factor exhibits a peak response of roughly 2 at 14 km.

Figure 5 shows that, within the MLSA, there is a secondary peak in the temperature response of 1.24. This local maximum occurs at the same altitude (~ 4 km) as the local stability minimum shown in Fig. 1. The coincidence of these two features suggests that, in response to a surface warming, the stability below the current 4 km stability minimum





ACPD
12, 11567–11594, 2012



will increase, while the stability above the current 4 km stability minimum will decrease. These stability changes are consistent with an upward displacement of the MLSA in a warmer atmosphere.

The gray curve in Fig. 5 shows the coefficient of determination ($r^2$) between the temperature anomalies at a particular height and the surface. The rapid decrease near 2 km in the strength of the coupling can presumably be attributed to a decrease in turbulence at the top of the boundary layer. In the rest of the troposphere, fluctuations in near surface temperature account for about a third of the variance in monthly mean temperatures.

The dashed black curve in Fig. 5 shows the amplification factor that would be expected from a temperature profile that was pseudoadiabatic at all altitudes. We first calculated the pseudoadiabatic temperature profiles associated with surface temperatures of 299.5 K and 300.5 K, using the assumptions discussed earlier, and set the amplification factor equal to the difference between the two profiles. The pseudoadiabatic amplification factor is significantly larger than the observed amplification factor at most heights, and does not reproduce the observed secondary maximum at 4 km.

### 3.4 Pressure response

We use the amplification factor shown in Fig. 5 to calculate the "warm" temperature profile that would be associated with a 1 °C increase in surface temperature. This requires some consideration of how the pressure profile responds to a surface warming. At each radiosonde location, for every month between 1998 and 2008, the vertical profile of the pressure anomaly can be calculated using the same procedure used to define the temperature anomaly. The change in pressure at each height, in response to a surface warming, can then be calculated from the slope of a scatter-plot of the pressure versus near surface temperature anomalies. Figure 6 shows the vertical profile of the pressure response (slope) associated with a 1 °C increase in near surface temperature (i.e. pressure amplification factor).





ACPD
12, 11567–11594, 2012



A warming and expansion of the atmospheric column implies a shift of the atmospheric center of mass to a higher altitude. At a fixed altitude, a warming of the atmosphere should be associated with an increase in the overhead column mass, and an increase in hydrostatic pressure. Figure 6 shows that pressure does indeed increase at most altitudes in response to a surface warming. This figure also shows, however, that the pressure below 3 km decreases.

The pressure decrease in the lower troposphere shown in Fig. 6 is probably a dynamical effect associated with the regional scale of the monthly warm anomalies. If the atmospheric warming is confined to the vicinity of the five radiosonde locations, the atmospheric center of mass would not rise to a higher altitude outside the radiosonde region, and positive pressure anomalies would not be expected. In this case, warm surface anomalies within the radiosonde region would be associated with high pressure anomalies aloft, relative to pressures on the same height surface outside the radiosonde region. These pressure anomalies would generate an outward divergent circulation (Maloney and Sobel, 2007) that would tend to export mass to the rest of the tropics, and reduce surface (and lower tropospheric) pressures within the radiosonde region.

The dashed gray curve in Fig. 6 shows the pressure response that would be expected in an atmosphere with a 1 °C surface warming in which: (i) the change in surface pressure was fixed at the observed value, (ii) the change in temperature was given by the amplification factor shown in Fig. 4, (iii) the relative humidity of the atmosphere was assumed fixed at the mean unperturbed value, and (iv) the change in pressure with height was calculated using hydrostatic balance with the virtual temperature calculated from (ii) and (iii). Because the two curves are essentially identical, the observed pressure response above the surface can be characterized as hydrostatic.

### 3.5 Warm lapse rate

The gray curve in Fig. 7 shows the "warm" lapse rate profile calculated from, (i) the temperature amplification factor shown in Fig. 2, (ii) the pressure amplification factor shown





ACPD
12, 11567–11594, 2012



in Fig. 6, and (iii) the height re-calculated from hydrostatic balance and constrained by the "warm" temperature versus pressure relationship. A running 3 point smoother has been applied to the "warm" lapse rate. The horizontal lines refer to the height of the melting level of the background (unperturbed) and "warm" temperature profiles. The MLSA of the warm profile has been displaced upward, by an amount roughly consistent with what would be expected from the upward displacement (~ 140 m) of the melting level.

### 3.6 CMIP models

This paper has used the relatively small monthly fluctuations in surface temperature within a convective region to characterize the vertical response of the atmosphere to a surface warming. There are several reasons for anticipating that this response may be different from the response to a surface warming that occurred on larger scales (i.e. tropical or global). In the tropics, as mentioned earlier, localized surface warmings are usually associated with dynamical feedbacks such as a local increase in precipitation, increased divergent outflow at upper levels, and a decrease in surface pressure. These dynamical feedbacks would be less likely to occur in response to surface warmings that occurred on a larger scale, and were associated with large scale increases in atmospheric temperature. The dynamical feedbacks expected to occur in association with localized surface temperature anomalies are likely to modify the observed temperature response. However, although the amplification factors calculated here on monthly timescales will not be identical to the amplification factors which occur on longer timescales, we use climate model simulations to show that the two amplification factors should be similar.

We calculated the temperature amplification factor of six models from the CMIP multi-model dataset, using a procedure that was as similar as possible to that used for the radiosonde dataset. We first identified the model grid columns closest to the five radiosonde stations. We then extracted the monthly mean temperature profiles and monthly mean rainfall rate at each location, from 1950 to 2000. The near surface tem-





ACPD
12, 11567–11594, 2012



perature anomaly was defined as the average anomaly of the first two levels. This was approximately equal to an average over the lowest 1 km. The temperature anomalies were then filtered using the same rainfall based criteria as used for the radiosondes.

The solid red and blue curves in Fig. 8 show the model mean amplification factor profiles for the 1990–2000 and 1950–2000 time periods. Although the amplification profile of the shorter time period is reduced in amplitude, the two profiles are similar.

Figure 8 also shows that the observed amplification profile is similar to the amplification profiles of the models. However, the models tend to underestimate the temperature response of the upper troposphere (10–16 km), and lack the secondary maximum at 4 km.

As mentioned earlier, the observed secondary maximum in the temperature response contributes to an upward displacement of the MLSA in response to a surface warming. The absence of this secondary maximum from the models can probably be attributed to the absence (for the most part) of a lapse rate feature resembling the observed MLSA. Figure 9 shows the climatological mean 1990–2000 lapse rate profiles of the six models, averaged over the five radiosonde grid columns, and the mean lapse rate profile of the radiosondes. Although the CCSM model shows a stability minimum at 4 km which is similar to the observed MLSA, this feature is not present in the other five models.

## 4 Discussion

The tropical mean amplification factor has been previously calculated from several radiosonde datasets. These datasets exhibit upper tropospheric peak amplification factors that, for the 1979–1999 period, range from near zero to larger than 2 (Santer et al., 2008). These differences arise mainly from differences in the methods used to remove measurement errors. The amplification profile calculated here is most consistent with those at the upper end of the observed range, which use the Radiosonde Observation Correction using Reanalyses (RAOBCORE) methodology (Haimberger et al., 2008).





ACPD
12, 11567–11594, 2012



It is important to keep in mind, however, that the temperature amplification factor calculated here is not directly comparable with previous estimates. For example, months with low rain rates, which give rise to a weak (or negative) correlation between surface and free tropospheric temperature anomalies, have been removed. This filtering will tend to increase the amplification factor in the troposphere. In addition, the radiosonde stations used here are located within a region where the average rainfall rate, and hence upward convective mass flux, are significantly larger than the tropical mean. The downward mass flux associated with radiative cooling is relatively uniform in the tropics. This implies that a rainfall enhancement within the radiosonde region will generate increased subsidence warming at larger scales, so that some of the induced temperature response will occur outside the radiosonde region. This effect will presumably decrease the amplification factor relative to one calculated for a larger convective region in which the mass budget is closer to being self contained. Finally, our amplification profile is calculated using monthly anomalies over an 11 yr period and is presumably smaller than one calculated using a longer term dataset.

The secondary maximum in the amplification factor factor at 4 km does not appear to have been observed previously, presumably due to a lack of vertical resolution in most radiosonde archives. The observed secondary minimum near the melting level may be related to a previously reported local minimum near 500 hPa in the temperature trend of a radiosonde dataset (Thorne et al., 2011).

The absence of a secondary maximum in the temperature response of the climate models can probably be attributed to their relatively poor spatial resolution, which requires that the effects of convective clouds and downdrafts on the background atmosphere be represented by parameterizations. However, this secondary maximum is also not represented (at least in the tropical mean response) in simulations using a high resolution cloud resolving model (Romps, 2011).





ACPD
12, 11567–11594, 2012



## 5 Conclusions

The height of the melting level in the tropics has risen by roughly ∼45 m over the past thirty years (Bradley et al., 2009). This rate of increase is quite modest. However, a change in the height of the melting level is likely to be associated with several important changes in tropical clouds and rainfall. These include a change in the cloud base altitude of precipitating stratiform clouds, an increase in the distance through which stratiform precipitation falls through cloud free air, an increase in the height of cumulus congestus clouds, a change in the vertical wavelength of the stratiform heating mode, and changes in the propagation of rainfall anomalies associated with convectively coupled equatorially trapped waves. Here, we provide indirect evidence that these changes are likely to occur in association with changes in the height of the melting level, by examining the change in lower tropospheric stability associated with monthly mean surface temperature anomalies from an actively convecting region in the tropics. If the MLSA is generated by mesoscale downdrafts below precipitating stratiform anvil clouds (Folkins, 2009), the upper boundary of the MLSA should shift to a higher altitude when surface temperatures increase. We find that this height increase does occur, and is roughly equal to the height increase of the melting level.

In an atmosphere in which the temperature profile followed a moist adiabat, the temperature amplification factor associated with a surface warming would increase monotonically with height, and reach a peak value of 3–4 in the upper troposphere. However, the radiosonde measurements analyzed here indicate a much more complex variation in the amplification factor with height. The amplification factor increases with height until 4 km, where it reaches a local maximum of 1.25. It then decreases with height and reaches a local minimum of roughly 1 slightly above the melting level. This variation of the amplification factor with height is associated with an upward shift in the height of the MLSA. Between 6 km and 10 km, where the atmospheric lapse rate is approximately pseudoadiabatic, the amplification factor again increases with height and reaches a value of roughly 2 near 14 km. Due to the complex response of temperatures in the





ACPD
12, 11567–11594, 2012



lower troposphere to changes in surface temperature, the large upper tropospheric amplification factors predicted by moist adiabatic ascent are not realized. Rather than monotonically increasing from 1 at the surface and peaking at 3–4 in the upper troposphere, the observed amplification factor monotonically increases from a value near 1 the melting level (~ 5 km) and peaks at a value of 2.

The temperature amplification profile calculated here was obtained from the monthly temperature fluctuations from an eleven year record of radiosonde observations. It is not clear that this profile should apply to climatic, as well as interannual, timescales. Comparisons with model results suggest, however, that the amplification profile obtained from a longer term radiosonde dataset should be similar to the profile calculated here.

The temperature amplification profile calculated here from the radiosonde observations is in better first order agreement with climate model simulations than most previous comparisons (Santer et al., 2005; Douglass et al., 2007). However, the climate models discussed here tend to under-estimate the temperature response of the upper troposphere, and do not simulate the secondary maximum in the amplification factor near 4 km.

*Acknowledgements.* This research was supported by the Natural Sciences and Engineering Research Council (NSERC). Some calculations were provided by Toni Mitovski. Glen Lesins is thanked for his input. We also acknowledge the modeling groups, the Program for Climate Model Diagnosis and Intercomparison (PCMDI), and the WCRP's Working Group on Coupled Modelling (WGCM), for their roles in making available the WCRP CMIP3 multi-model dataset. Support of this dataset is provided by the Office of Science, U.S. Department of Energy.

## References

Adler, R. F., Huffman, G. J., Bolvin, D. T., Curtis, S., and Nelkin, E. J.: Tropical rainfall distributions determined using TRMM combined with other satellite and rain gauge information, J. Appl. Meteorol., 39, 2007–2023, 2000. 11574





ACPD

12, 11567–11594, 2012



Bradley, R. S., Keimig, F., Diaz, H., and Hardy, D.: Recent changes in freezing level heights in the tropics with implications for the deglacierization of high mountain regions, Geophys. Res. Lett., 36, L17701, doi:10.1029/2009GL037712, 2009. 11568, 11581

Chiang, J. C. H. and Lintner, B. R.: Mechanisms of remote tropical surface warming during El Nino, J. Climate, 18, 4130–4149, 2005. 11574

Douglass, D. H., Christy, J. R., Pearsona, B. D., and Singer, S. F.: A comparison of tropical temperature trends with model predictions, Int. J. Climatol., 28, 1693–1701, doi:10.1002/joc.1651, 2007. 11582

Emanuel, K. A.: Atmospheric Convection, Oxford University Press, New York, USA, 1994. 11570

Folkins, I.: Convective damping of buoyancy anomalies and its effect on lapse rates in the tropical lower troposphere, Atmos. Chem. Phys., 6, 1–12, doi:10.5194/acp-6-1-2006, 2006. 11573

Folkins, I.: A one-dimensional cloud model with trimodal convective outflow, J. Climate, 22, 6437–6455, 2009. 11569, 11581

Folkins, I., Fueglistaler, S., Lesins, G., and Mitovski, T.: A low-level circulation in the tropics, J. Atmos. Sci., 65, 1019–1034, 2008. 11574

Haimberger, L., Tavolato, C., and Sperka, S.: Towards elimination of the warm bias in historic radiosonde records – some new results from a comprehensive intercomparison of upper air data, J. Climate, 21, 4587–4606, doi:10.1175/2008JCLI1929.1, 2008. 11579

Houze, R. A., Jr.: Mesoscale convective systems, Rev. Geophys., 42, RG4003, doi:10.1029/2004RG000150, 2004. 11568

Johnson, R. H., Rickenbach, T. M., Rutledge, S. A., Ciesielski, P. E., and Schubert, W. H.: Trimodal characteristics of tropical convection, J. Atmos. Sci., 12, 2397–2418, 1999. 11570, 11573

Kiladis, G. N., Wheeler, M. C., Haertal, P. T., Straub, K. H., and Roundy, P. E.: Convectively coupled equatorial waves, Rev. Geophys., 47, RG2003, doi:10.1029/2008RG000266, 2009. 11569

Kummerow, C., Simpson,J., Thiele, O., Barnes, W., Chang, A. T. C., Stocker, E., Adler, R. F., Hou, A., Kakar, R., Wentz, F., Ashcroft, P., Kozu, T., Hong, Y., Okamoto, K., Iguchi, T., Kuroiwa, H., Im, E., Haddad, Z., Huffman, G., Krishnamurti, T., Ferrier, B., Olson, W. S., Zipser, E., Smith, E. A., Wilheit, T. T., North, G., and Nakamura, K.: The status of the tropical





ACPD
12, 11567–11594, 2012



rainfall measuring mission (TRMM) after two years in orbit, J. Appl. Meteorol., 39, 1965–1982, 2000. 11572
Maloney, E. D. and Sobel, A. H.: Idealized hot spot experiments with a general circulation model, J. Climate, 20, 908–925, 2007. 11577
Mapes, B. E.: Water's two scale heights: The moist adiabat and the radiative troposphere, Q. J. Roy. Meteorol. Soc., 127, 2353–2366, 2001. 11569, 11573
Mapes, B. E. and Houze, R. A.: Diabatic divergence profiles in Western Pacific mesoscale convective systems, J. Atmos. Sci., 52, 1807–1828, 1995. 11569
McPhaden, M. J.: Genesis and evolution of the 1997–98 El Nino, Science, 283, 950–954, doi:10.1126/science.283.5404.950, 1999. 11574
Meehl, G. A., Covey, C., Delworth, T., Latif, M., McAvaney, B., Mitchell, J. F. B., Stouffer, R. J., and Taylor, K. E.: The WCRP CMIP3 multi-model dataset: a new era in climate change research, B. Am. Meteorol. Soc., 88, 1383–1394, 2007. 11571
Mitovski, T., Folkins, I., Martin, R. V., and Cooper, M.: Testing convective transport on short time scales: comparisons with mass divergence and ozone anomaly patterns about high rain events, J. Geophys. Res., 117, D02109, doi:10.1029/2011JD016321, 2012. 11570
Randel, W. J. and Wu, F.: Biases in stratospheric and tropospheric temperature trends derived from historical radiosonde data, J. Climate, 19, 2094–2104, 2006. 11570
Redelsperger, J. L., Parsons, D. B., and Guichard, F.: Recovery processes and factors limiting cloud-top height following the arrival of a dry intrusion observed during TOGA-COARE, J. Geophys. Res., 59, 2438–2457, 2002. 11570
Romps, D.: Response of tropical precipitation to global warming, J. Atmos. Sci., 68, 123–139, 2011. 11580
Santer, B. D., Wigley, T. M. L., Mears, C., Wentz, F. J., Klein, S. A., Seidel, D. J., Taylor, K. E., Thorne, P. W., Wehner, M. F., Gleckler, P. J., Boyle, J. S., Collins, W. D., Dixon, K. W., Doutriaux, C., Free, M., Fu, Q., Hansen, J. E., Jones, G. S., Ruedy, R., Karl, T. R., Lanzante, J. R., Meehl, G. A., Ramaswamy, V., Russell, G., and Schmidt, G. A.: Amplification of surface temperature trends and variability in the tropical atmosphere, Science, 309, 1551–1556, doi:10.1126/science.1114867, 2005. 11582
Santer, B. D., Thorne, P. W., Haimberger, L., Taylor, K. E., Wigley, T. M. L., Lanzante, J. R., Solomon, S., Free, M., Gleckler, P. J., Jones, P. D., Karl, T. R., Klein, S. A., Mears, C., Nychka, D., Schmidt, G. A., Sherwood, S. C., and Wentz, F. J.: Consistency of modeled and





ACPD
12, 11567–11594, 2012



observed temperature trends in the tropical troposphere, Int. J. Climatol., 28, 1703–1722, doi:10.1002/joc.1756, 2008. 11579

Sherwood, S. C., Lanzante, J., and Meyer, C.: Radiosonde daytime biases and late 20th Century warming, Science, 309, 1556–1559, doi:10.1126/science.1115640, 2005. 11570

Thorne, P. W., Brohan, P., Titchner, K. A., McCarthy, M. P., Sherwood, S. C., Peterson, T. C., Haimberger, L., Parker, D. E., Tett, S. F. B., Santer, B. D., Fereday, D. R., and Kennedy, J. J.: A quantification of uncertainties in historical tropical tropospheric temperature trends from radiosondes, J. Geophys. Res., 116, D12116, doi:10.1029/2010JD015487, 2011. 11570, 11580

Tokay, A., Short, D. A., Williams, C. R., Ecklund, W. L., and Gage, K. S.: Tropical rainfall associated with convective and stratiform clouds: intercomparison of disdrometer and profiler measurements, J. Appl. Meteorol., 38, 302–320, 1999. 11568





ACPD

12, 11567–11594, 2012



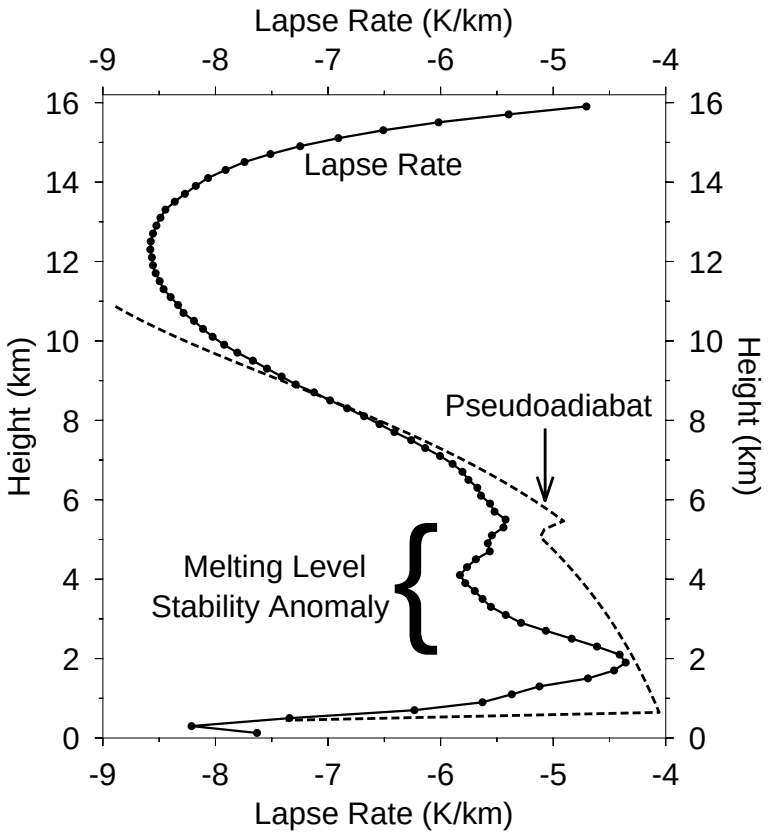


**Fig. 1.** The solid curve with bullets shows the mean lapse rate profile (1998–2008) of the five radiosonde stations discussed in this paper. The dashed curve shows the lapse rate profile of a parcel starting from the surface with a temperature of 299.5 K and relative humidity of 80 %, and subjected to pseudoadiabatic ascent.





ACPD
12, 11567–11594, 2012



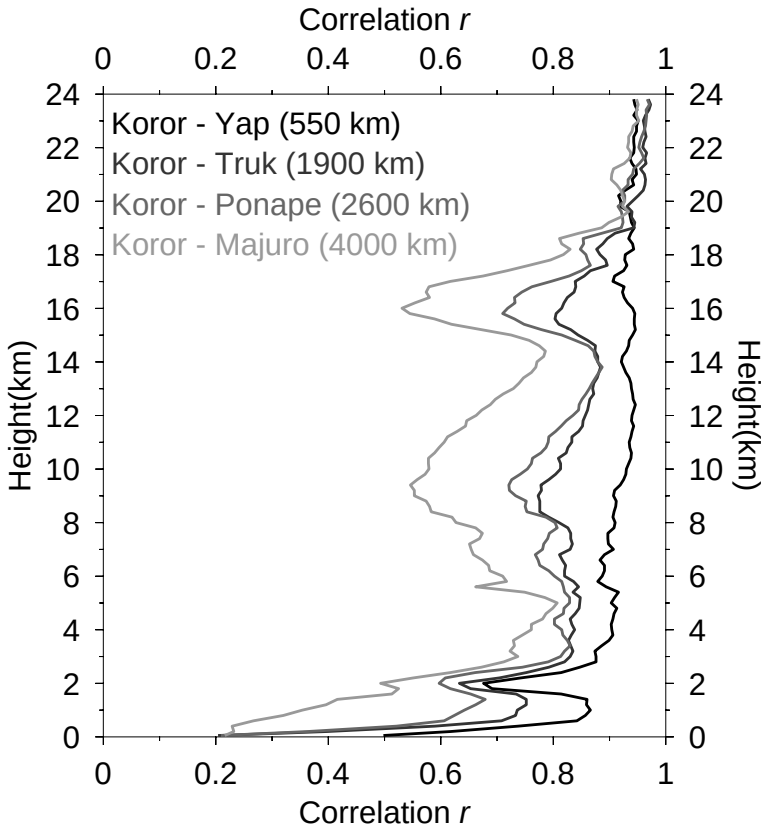


**Fig. 2.** Vertical profiles of the correlation coefficients between monthly temperature anomalies at Koror and four other radiosonde stations. The correlation coefficient decreases as the distance between the radiosonde stations increases. However, due to the tendency of temperature fluctuations in the tropics to have a large spatial scale, radiosonde stations as far apart as 4000 km are quite strongly correlated.





ACPD
12, 11567–11594, 2012



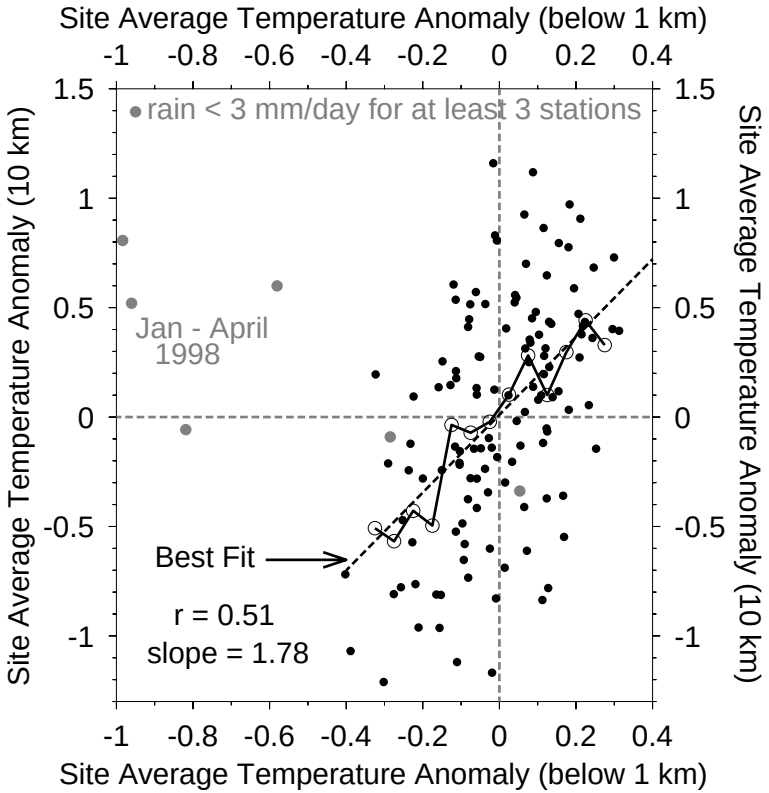


**Fig. 3.** The black dots are a scatterplot of the monthly mean 10 km temperature anomaly versus the monthly mean surface temperature anomaly (below 1 km), averaged over all five radiosonde stations. The dashed line shows a best fit, while the solid line with open circles shows the mean 10 temperature anomaly as a function of the surface temperature anomaly. The gray dots indicate temperature anomaly pairs during which the mean rainfall rate was less than 3 mm per day, at three of the five radiosonde stations. Four of these six months occurred during the first four months of 1998, during which the surface cooling was larger than −0.6 °C.





ACPD
12, 11567–11594, 2012



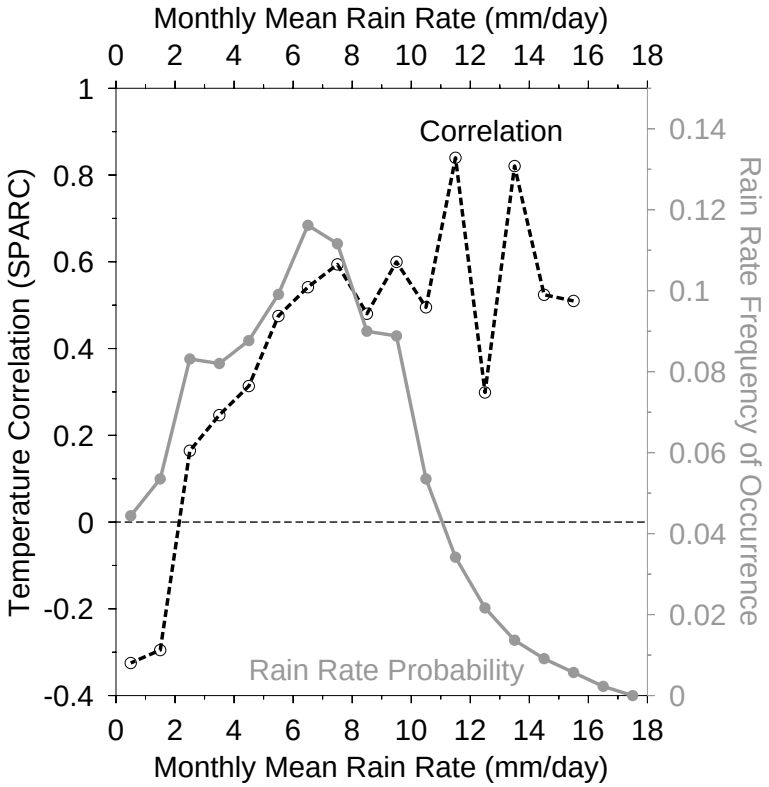


**Fig. 4.** The dashed curve shows the strength of the correlation between the near surface (below 1 km) and 10 km monthly mean temperature anomalies of a radiosonde station, as a function of the average rain rate in a 2° × 2° box centered at each station. The solid gray curve shows the normalized probability of a particular monthly mean rain rate being observed at one of the five radiosonde stations.





ACPD
12, 11567–11594, 2012



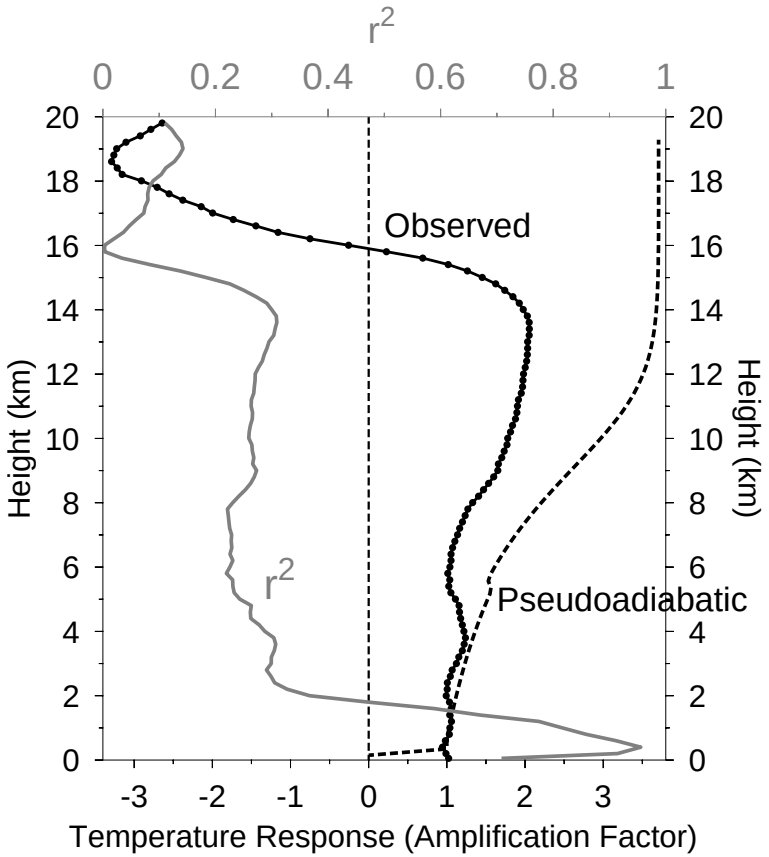


**Fig. 5.** The solid curve with bullets shows the observed temperature amplification factor profile (i.e. temperature response associated with a 1 °C increase in surface temperature). The dashed curve shows the amplification factor of an atmosphere with a pseudoadiabatic lapse rate. The solid gray curve shows the coefficient of determination ($r^2$) between temperatures fluctuations near the surface (below 1 km) and temperature fluctuations aloft.





ACPD
12, 11567–11594, 2012



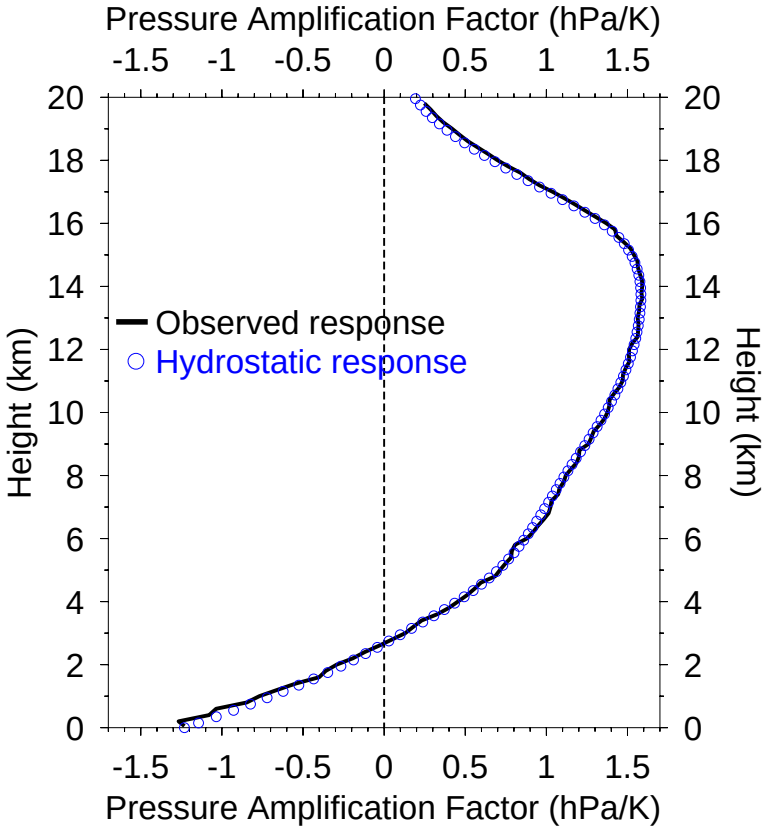


**Fig. 6.** The solid curve shows the change in pressure as a function of height, associated with a 1 ˚C increase in near surface temperature. It was derived from a slope of a scatterplot, at each height, of the monthly mean pressure anomaly against the monthly mean near surface temperature anomaly. The blue open circles show the pressure response expected from hydrostatic balance, constrained by the observed pressure change at the surface.





ACPD
12, 11567–11594, 2012



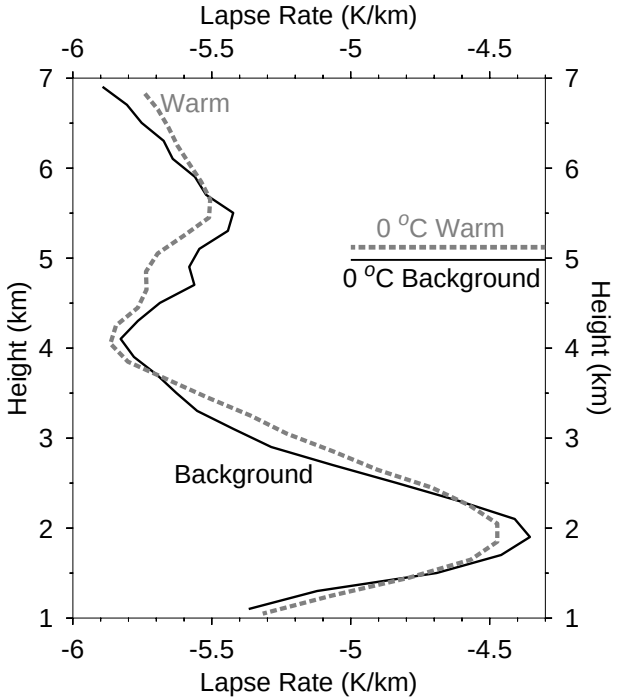


**Fig. 7.** The black solid curve shows the average lapse rate of the five radiosonde stations during the 11 yr period (1998–2008). The dashed gray curve is the "warm" lapse rate of a temperature profile subjected to a 1 °C increase in near surface temperature, as described in the text. Surface warming is associated with a shift in the lapse rate profile to a higher altitude, by an amount roughly equal to the displacement in the melting level.





ACPD
12, 11567–11594, 2012



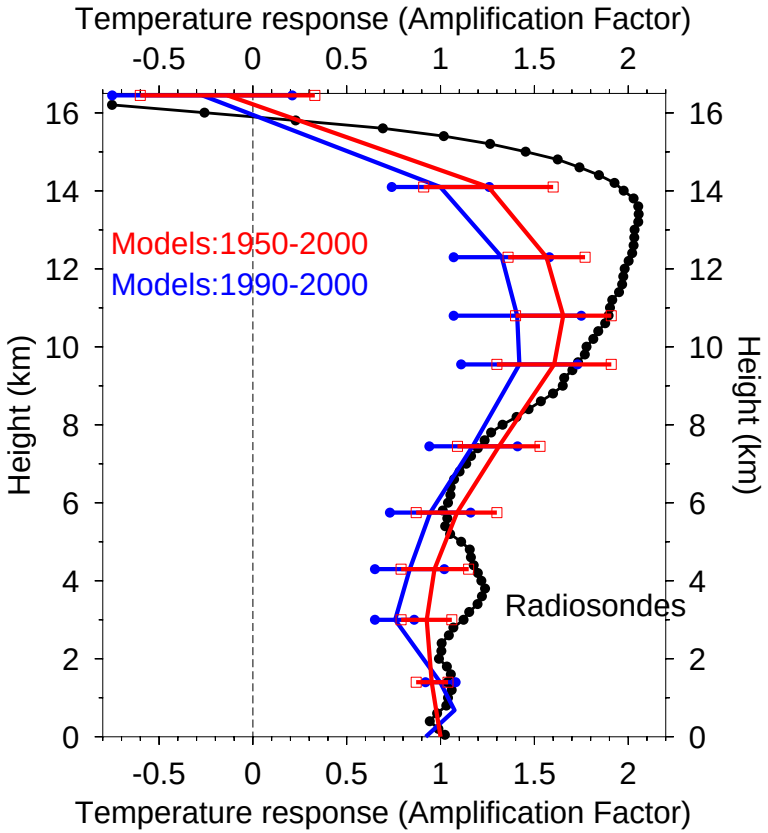


**Fig. 8.** The black curve shows the observed temperature amplification factor (as shown earlier in Fig. 5). The red and blue curves show the model mean 1950–2000 and 1990–2000 amplification factors, respectively. The widths of the model curves are equal to twice the average difference of the 6 model runs from the model mean.





ACPD
12, 11567–11594, 2012



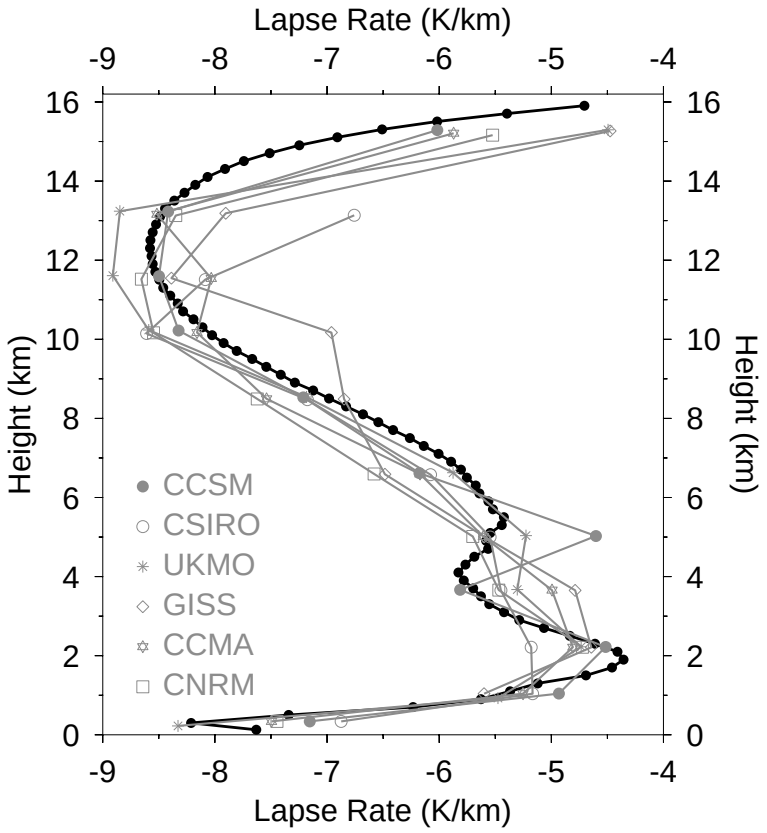


**Fig. 9.** The black solid curve shows the average lapse rate of the five radiosonde stations during the 11 yr period (1998–2008), as previously shown in Fig. 1. Gray curves refer to mean lapse rates of particular models.





ACPD
12, 11567–11594, 2012

Height increase of the melting level stability anomaly

I. Folkins